CHALMERS
UNIVERSITY OF TECHNOLOGY

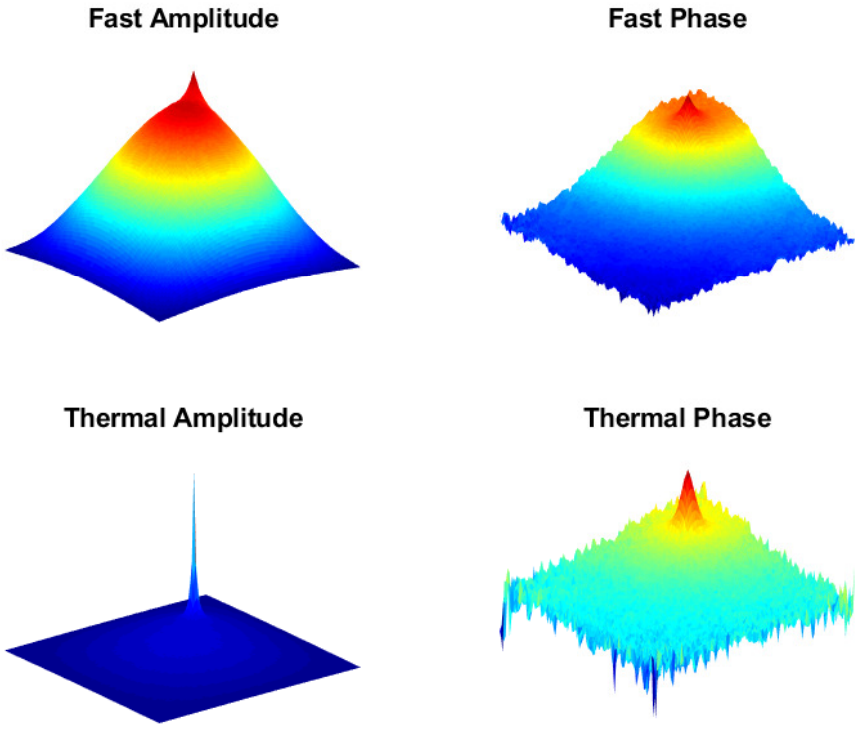

Modelling the Effect of Stationary Fluctuations in Nuclear Reactors Using Probabilistic Methods

A Monte-Carlo Based Method for Calculating the Effect of Stationary Fluctuations in 1D and 2D Systems

Master's thesis in Nuclear Science and Technology

ANDREAS TATIDIS

Department of Physics
CHALMERS UNIVERSITY OF TECHNOLOGY
Gothenburg, Sweden 2019
CTH-NT-338

CTH-NT-338

Master's thesis 2019:57124

Modelling the Effect of Stationary Fluctuations in Nuclear Reactors Using Probabilistic Methods

A Monte-Carlo Based Method for Calculating the Effect of Stationary Fluctuations in 1D and 2D Systems

Andreas Tatidis

CHALMERS
UNIVERSITY OF TECHNOLOGY

Department of Physics
Division of Subatomic Physics and Plasma Physics
Chalmers University of Technology
Gothenburg, Sweden 2019

Modelling the Effect of Stationary Fluctuations in Nuclear Reactors Using Probabilistic Methods
A Monte-Carlo Based Method for Calculating the Effect of Stationary Fluctuations in 1D and 2D Systems
ANDREAS TATIDIS

Supervisor: Chistophe DEMAZIERE, Chalmers, Department of Physics
Examiner: Chistophe DEMAZIERE, Chalmers, Department of Physics

Master's Thesis 2019:57124
Department of Physics, CTH-NT-338
Division of Subatomic Physics and Plasma Physics
Chalmers University of Technology
SE-412 96 Gothenburg

Cover: Off-centre perturbation in homogeneous square reactor at $10/2\pi$ Hz

Typeset in LaTeX
Gothenburg, Sweden 2019

Modelling the Effect of Stationary Fluctuations in Nuclear Reactors Using Probabilistic Methods
Monte-Carlo Based Method for Calculating the Effect of Stationary Fluctuations in 1D and 2D
ANDREAS TATIDIS
Department of Physics
Chalmers University of Technology

Abstract

A Monte-Carlo-based method for determining the effect on the neutron flux of stationary fluctuations in 1D and 2D is proposed in this study. The cross-sections of the two-group balance equations relying on the diffusion approximation in the frequency domain are split into their real and imaginary parts, and a modified Green's function technique is used. In this technique, the balance equations for the real part of the balance equations are mimicked with Monte Carlo using an equivalent subcritical system. The exact same balance equations are obtained for the imaginary part. The coupling between the real and imaginary parts are resolved outside of the Monte Carlo Code, taking advantage of the properties of the Green's function. The amplitude and phase close to the point of perturbation agree well with diffusion based-codes such as CORE SIM. This method is applicable to any frequency, and any type of cross-section perturbation. The Green's function is furthermore found to be insensitive to frequencies around and above the plateau region. Using the Green's function at one given frequency within this frequency range has thus a negligible impact on the estimated fluctuations in neutron flux.

Keywords: Neutron noise, Monte Carlo, diffusion theory, Green's function

Acknowledgements

Thanks to Eirik Eide Pettersen for his previous work [1, 2] and for sending his files.

Andreas Tatidis, Gothenburg, April 2019

Contents

List of Figures

List of Tables

1
Introduction

Today, the fleet of nuclear reactors in operation in Europe is getting close to the end of its lifetime. More than 60% of the reactors in operation are over 30 years old and due to ageing of the reactor vessels and material stresses more problems are expected to occur. Furthermore, the conservatism in nuclear safety analyses has been reduced as the tools available today have an increased fidelity and refinement. For these reasons there is a need today for better core monitoring techniques to early detect any possible unexpected core behaviour.

Nuclear reactor systems, even at steady-state conditions, display fluctuations in neutron flux around their mean value. Such fluctuations are referred to as "noise" and arise due to the turbulent flow, the presence of boiling, mechanical vibrations, and the stochastic nature of the nuclear reactions taking place in the core. The mean values representative of the steady-state are, in most cases, more important than the fluctuations. However, the fluctuations contain information about the dynamics of the system and are of great importance for diagnostic purposes when determining e.g. the possible location of perturbations in the system that cause fluctuations of the neutron flux in the system [3].

Despite the stochastic nature of the driving fluctuations, the modelling of the noise is mostly performed with deterministic models [4, 5, 6, 7, 8]. In such models, multi-group diffusion theory is used to derive balance equations, those equations are split into a mean value and a fluctuating part, and Fourier transformed since the noise sources tend to be stationary. The static solution is used to estimate the multiplication factor, k_{eff}, as well as the static flux. The main reason to use Monte Carlo codes instead of the more used deterministic codes is that Monte Carlo tends to use fewer approximations, and describes the space-dependence of a system with more details independently of mesh size and size of the system.

An earlier project at the Division of Subatomic and Plasma Physics, Department of Physics, Chalmers University of Technology aimed to demonstrate the feasibility of using Monte Carlo code by splitting the balance equations into real and imaginary parts [2, 1]. This project coupled diffusion theory with the Monte Carlo simulations by using custom cross-sections representing multi-group diffusion theory according to [9]. This model, when performing the simulations, ignored the coupling between the imaginary and real parts which means that the simulations could only be performed for frequencies that yield fluctuations with a purely real or purely imaginary part. For frequencies with both real and imaginary contributions, iteration between the real and imaginary parts would need to be performed, calculating each part separately until convergence. Furthermore, the developed model was unable to handle possible negative contributions in the real or imaginary parts

of the balance equations. Although not stated in that report, ignoring the coupling between real and imaginary components has the repercussion that the model does not work for high frequencies, since by ignoring the coupling the neutron speed dependent terms are also ignored. Such terms are the main contributing terms for high frequency perturbations. The previous model is furthermore unable to estimate the fluctuating flux for frequencies where both the real and imaginary parts have significant contributions due to the absence of the coupling. That means that the model works for low frequencies $f \lesssim 0.005\,\mathrm{Hz}$ where the phase is expected to be $-\pi/2\,\mathrm{rad}$ or $f \approx 1\,\mathrm{Hz}$ where the phase is expected to be $0\,\mathrm{rad}$, as explained in section 2.2.

A different approach is hereafter presented here that makes it possible to determine the noise at any frequency without any modification to the existing Monte Carlo source codes. This is made possible by splitting only the cross-section matrix into its real and imaginary part and acting upon the imaginary cross-sections as an external source. The real part of the cross-sections are used to determine a modified Green's function, which is estimated with Monte Carlo code, and then the noise is determined by taking advantage of the Green's function technique.

The Monte Carlo code used for this project is MCNP6.2 [10]. For this method, as of the writing of this report, the Monte Carlo code Serpent 2.1.19 [11] has been proven to be incapable of being modified in the desired manner [12], because Serpent expects the first interaction to be an elastic scattering which is formally not defined in this present method.

Although the time required to perform such Monte Carlo simulations is long, once the Green's function is obtained, the estimation of the induced neutron noise can be done in seconds, which speaks for its usefulness.

2

Theory

2.1 Balance Equations & Green's Function

The neutron flux, $\boldsymbol{\phi}$, is here defined by the time-dependent two-group diffusion equation as:

$$\begin{bmatrix} \frac{1}{v_1}\frac{\partial}{\partial t} & 0 \\ 0 & \frac{1}{v_2}\frac{\partial}{\partial t} \end{bmatrix} \boldsymbol{\phi} = \nabla \cdot \begin{bmatrix} D_{1,0} & 0 \\ 0 & D_{2,0} \end{bmatrix} \nabla \boldsymbol{\phi} + \begin{bmatrix} (1-\beta)\nu\Sigma_{f,1} - \Sigma_{a,1} - \Sigma_r & (1-\beta)\nu\Sigma_{f,2}) \\ \Sigma_r & -\Sigma_{a,2} \end{bmatrix} \boldsymbol{\phi} + \begin{bmatrix} \lambda C \\ 0 \end{bmatrix} \quad (2.1)$$

where the flux, cross sections and concentration of precursors are dependent on time and space, the diffusion coefficients are dependent only on space, as neglecting the time-dependence has no impact for practical noise calculations[7]. The term of the left hand side describes the time dependence of the flux, the first term on the right side describes how the neutrons diffuse and leak out of the system, the second term describes all the neutron interactions that can occur and the last term describes the neutron contribution from decaying fission products. The flux matrix, $\boldsymbol{\phi} = [\phi_1, \phi_2]^\intercal$, contains both the fast and thermal components and has the size $2N \times N$, where N is the size of the fast and thermal fluxes, respectively, originating from the spatial discretization of the equations. Each cross-section Σ is a diagonal matrix of the size N, and the thermal component contian neutrons with energies below 0.625 eV while the fast component contains neutrons above 0.625 eV. The equation for one-group of precursors of delayed neutrons, C, is defined as:

$$\frac{\partial}{\partial t} C = \beta\nu\Sigma_{f,1}\phi_1 + \beta\nu\Sigma_{f,2}\phi_2 - \lambda C, \quad (2.2)$$

where the left hand side describes the time-dependence of the precursors, the first and second terms of the right side describe the production of precursors resulting from fission in the fuel and the last term describes the decay of the concentration of precursors. The removal cross-section is defined as:

$$\Sigma_r = \Sigma_{s0,1\to2} - \Sigma_{s0,2\to1}\phi_2/\phi_1, \quad (2.3)$$

and describes the exchange of neutrons between energy groups.

All time-dependent quantities, $X(\mathbf{r}, t)$, are split into a time-independent mean, $X_0(\mathbf{r})$, and a fluctuating part $\delta X(\mathbf{r}, t)$, Fourier transformed in time and the second order fluctuations, assumed to be small, are ignored. The derivation of the noise

diffusion equation assumes that the reactor is operating at steady-state conditions. To ensure such a condition and to avoid any deviation from it due to the spatial discretization, the fission cross-sections are re-normalised according to: $\nu\Sigma_{f,g} = \nu\Sigma_{f,g}/k_{eff}$. The static part of the diffusion equation thus becomes

$$\nabla \cdot \begin{bmatrix} D_{1,0} & 0 \\ 0 & D_{2,0} \end{bmatrix} \nabla \boldsymbol{\phi}_0 + \begin{bmatrix} \frac{\nu\Sigma_{f,1,0}}{k_{eff}} - \Sigma_{a,1,0} - \Sigma_{r,0} & \frac{\nu\Sigma_{f,2,0}}{k_{eff}} \\ \Sigma_{r,0} & -\Sigma_{a,2,0} \end{bmatrix} \boldsymbol{\phi}_0 = 0, \tag{2.4}$$

and the dynamic part is

$$\nabla \cdot \mathbf{D}\nabla\boldsymbol{\delta\phi} + \boldsymbol{\Sigma}\boldsymbol{\delta\phi} = -\boldsymbol{\delta S} \tag{2.5}$$

where the matrices are defined as:

$$\mathbf{D} = \begin{bmatrix} D_{1,0} & 0 \\ 0 & D_{2,0} \end{bmatrix} \tag{2.6}$$

$$\boldsymbol{\Sigma} = \begin{bmatrix} \frac{\nu\Sigma_{f,1,0}}{k_{eff}}\left(1 - \frac{i\omega\beta}{i\omega+\lambda}\right) - \frac{i\omega}{v_1} - \Sigma_{a,1,0} - \Sigma_{r,0} & \frac{\nu\Sigma_{f,2,0}}{k_{eff}}\left(1 - \frac{i\omega\beta}{i\omega+\lambda}\right) \\ \Sigma_{r,0} & -\frac{i\omega}{v_2} - \Sigma_{a,2,0} \end{bmatrix} \tag{2.7}$$

$$\boldsymbol{\delta S} = \begin{bmatrix} \frac{\delta\nu\Sigma_{f,1}}{k_{eff}}\left(1 - \frac{i\omega\beta}{i\omega+\lambda}\right) - \delta\Sigma_{a,1} - \delta\Sigma_r & \frac{\delta\nu\Sigma_{f,2}}{k_{eff}}\left(1 - \frac{i\omega\beta}{i\omega+\lambda}\right) \\ \delta\Sigma_r & -\delta\Sigma_{a,2} \end{bmatrix} \boldsymbol{\phi}_0. \tag{2.8}$$

The normal procedure to solve these equations is to first solve the static one to obtain the static flux, $\boldsymbol{\phi}_0$, and the multiplication factor, k_{eff}, and then update the cross-sections, $\boldsymbol{\Sigma}$ & $\boldsymbol{\delta\Sigma}$, with these values before solving the dynamic equation. However, Monte Carlo can not interpret complex valued cross-section since the complex values do not have a direct physical meaning. A way to work around this problem is to split the cross-section matrix, (2.7), in the dynamic equation into its real, $\boldsymbol{\Sigma}^R$, and imaginary part, $\boldsymbol{\Sigma}^I$, move the imaginary cross-sections to the right hand side and redefine the source term as

$$\nabla \cdot \mathbf{D}\nabla\boldsymbol{\delta\phi} + \boldsymbol{\Sigma}^R\boldsymbol{\delta\phi} = -\boldsymbol{\delta S} - i\boldsymbol{\Sigma}^I\boldsymbol{\delta\phi} = -\mathbf{S}, \tag{2.9}$$

where

$$\boldsymbol{\Sigma^R} = \begin{bmatrix} \frac{\nu\Sigma_{f,1,0}}{k_{eff}}\frac{\lambda^2+\omega^2(1-\beta))}{\lambda^2+\omega^2} - \Sigma_{a,1,0} - \Sigma_{r,0} & \frac{\nu\Sigma_{f,2,0}}{k_{eff}}\frac{\lambda^2+\omega^2(1-\beta))}{\lambda^2+\omega^2} \\ \Sigma_{r,0} & -\Sigma_{a,2,0} \end{bmatrix} \tag{2.10}$$

$$\boldsymbol{\Sigma^I} = \begin{bmatrix} -\frac{\nu\Sigma_{f,1,0}}{k_{eff}}\frac{\omega\beta\lambda}{\lambda^2+\omega^2} - \frac{\omega}{v_1} & -\frac{\nu\Sigma_{f,2,0}}{k_{eff}}\frac{\omega\beta\lambda}{\lambda^2+\omega^2} \\ 0 & -\frac{\omega}{v_2} \end{bmatrix}. \tag{2.11}$$

Now all the real valued parameters are on the left hand side of (2.9), while the right hand side contains complex valued parameters. Therefore, by using the Green's function technique, the Green's function of this modified neutron noise diffusion equation is given by

$$\nabla \cdot \mathbf{D}\nabla \begin{bmatrix} G_{1\to1}(\mathbf{r},\mathbf{r}',\omega) \\ G_{1\to2}(\mathbf{r},\mathbf{r}',\omega) \end{bmatrix} + \boldsymbol{\Sigma}^R \begin{bmatrix} G_{1\to1}(\mathbf{r},\mathbf{r}',\omega) \\ G_{1\to2}(\mathbf{r},\mathbf{r}',\omega) \end{bmatrix} = - \begin{bmatrix} \delta(\mathbf{r}-\mathbf{r}') \\ 0 \end{bmatrix}, \tag{2.12}$$

and

$$\nabla \cdot \mathbf{D}\nabla \begin{bmatrix} G_{2\to1}(\mathbf{r},\mathbf{r}',\omega) \\ G_{2\to2}(\mathbf{r},\mathbf{r}',\omega) \end{bmatrix} + \boldsymbol{\Sigma}^R \begin{bmatrix} G_{2\to1}(\mathbf{r},\mathbf{r}',\omega) \\ G_{2\to2}(\mathbf{r},\mathbf{r}',\omega) \end{bmatrix} = - \begin{bmatrix} 0 \\ \delta(\mathbf{r}-\mathbf{r}') \end{bmatrix}. \tag{2.13}$$

All values in these equations are real and the equations resemble a static equation with an external source. Therefore, the Green's function can be estimated with Monte Carlo code, by acting upon the Dirac delta functions as if they were external sources and by inputing the correct real valued cross-sections, $\boldsymbol{\Sigma}^R$, to the problem. The dynamic flux is then given by the integral equation

$$\boldsymbol{\delta\phi}(\mathbf{r},\omega) = \int_V G(\mathbf{r},\mathbf{r}',\omega)\left(\boldsymbol{\delta S}(\mathbf{r}',\omega) + i\boldsymbol{\Sigma}^I\boldsymbol{\delta\phi}(\mathbf{r}',\omega)\right)\mathrm{d}V', \tag{2.14}$$

which is a Fredholm equation of the second kind, with the Green's function defined as

$$G = \begin{bmatrix} G_{1\to1} & G_{2\to1} \\ G_{1\to2} & G_{2\to2} \end{bmatrix}, \tag{2.15}$$

where the first index, g, of $G_{g\to g'}$ describes which energy group the neutron source emits neutrons in and the second index, g', describes in which energy group the neutron is absorbed in.

The frequency dependent factor when splitt into its real and imaginary parts is equal to

$$1 - \frac{i\omega\beta}{i\omega+\lambda} = \frac{\lambda^2+\omega^2(1-\beta)}{\lambda^2+\omega^2} + i\frac{\omega\lambda\beta}{\lambda^2+\omega^2}. \tag{2.16}$$

It is seen that the real part is bound between 1 and $1-\beta$ and that it is close to its lower limit for frequencies at the plateau region or for frequencies above $f \gtrsim 1\,\mathrm{Hz}$, with an relative error of $\sim 10^{-6}$, that is for frequencies $\omega >> \lambda$ the real part of the frequency-dependent factor is asymptotically equal to a constant

$$\frac{1}{k_{eff}}\frac{\lambda^2+\omega^2(1-\beta)}{\lambda^2+\omega^2} \simeq \frac{1-\beta}{k_{eff}}. \tag{2.17}$$

The imaginary part, on the other hand, is zero at low or high frequencies outside of the plateau region. Furthermore, The Green's function, since it is determined by the real valued cross-sections, has a weak frequency dependence for values on the plateau and above, which means that the Green's frequency can be fixed at $\sim$1 Hz and the dynamic flux will be valid for any frequency from 1 Hz to ∞ Hz.

2.2 Stationary Noise Fluctuation Basics

A typical transfer function for neutron noise in light water reactors, according to the point kinetic model [3], is described by the zero-power reactor transfer function:

$$G_0(\omega) = \frac{1}{i\omega\left(\Lambda + \frac{\beta}{i\omega+\lambda}\right)}, \tag{2.18}$$

λ is the precursor decay constant describing the decay rate of fission products that emit neutrons, Λ, the mean prompt neutron lifetime and, β, the delayed neutron fraction, and its Bode diagram is displayed in figure 2.1. Typical values for these quantities are $\lambda \approx 0.0851\,\mathrm{s}^{-1}$, $\Lambda \approx 0.1\,\mathrm{ms}$ and $\beta \approx 530\,\mathrm{pcm}$ (per cent mille). For low frequencies, $f \lesssim 0.005\,\mathrm{Hz}$, and high frequencies, $f \gtrsim 500\,\mathrm{Hz}$, the same behaviour concerning the phase is obtained, both having similar time delays. At frequencies around 1 Hz, at the plateau region, the phase is close to zero meaning that there is no delay in the response. The lower and upper cut-offs for this transfer function are at the $\lambda/2\pi\,\mathrm{Hz}$ and $\beta/\Lambda 2\pi\,\mathrm{Hz}$, respectively. At these points, the real and imaginary parts of the dynamic fluxes are of the same order making these regions especially interesting from a computational point of view. Therefore these cut-off points have been chosen for the comparison with CORE SIM.

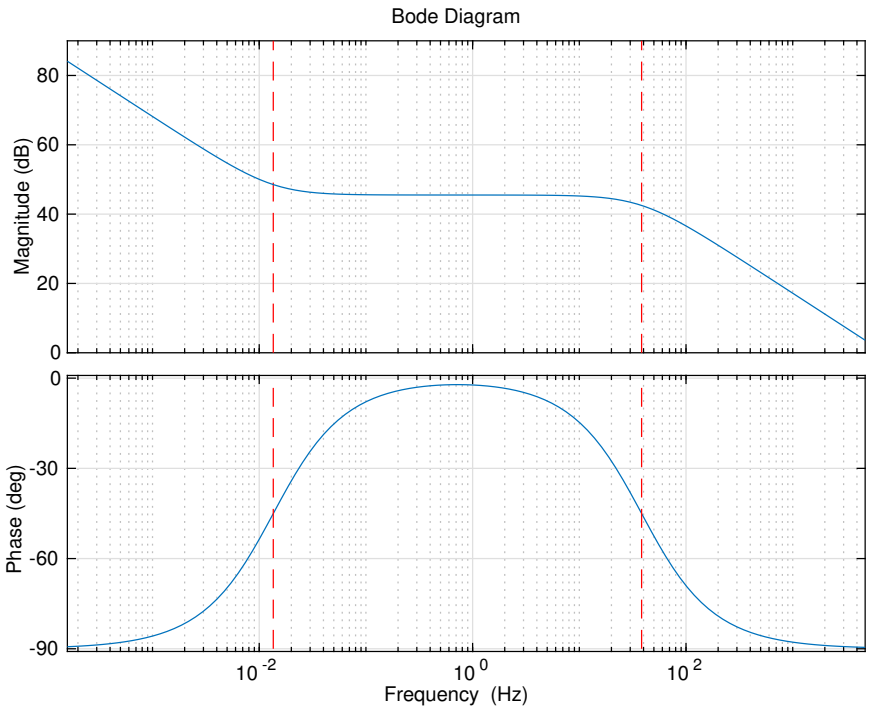

Figure 2.1: Typical zero-power reactor transfer function for light water reactors according to the point kinetic model, with cut-offs at $\lambda/2\pi\,\mathrm{Hz}$ and $\beta/\Lambda 2\pi\,\mathrm{Hz}$.

2.3 Discretization of Integral Equation

The discretization of the integral equation for the one dimensional case is done as followed. x is represented by the index n and x' by the index m. As a result, the flux is represented as $\delta\phi(x) = \delta\phi_n$ and the Green's function as $G_{g\to g'}(x, x') = G_{g\to g',nm}$, with a mesh size of N. Element wise, the integral equation in one dimension is

$$\delta\phi_n = \sum_m \int_L G_{nm} \left(\delta S_m + i[\Sigma^I \delta\phi]_m\right) \mathrm{d}x', \tag{2.19}$$

$L \in [a, b]$ and$[\Sigma^I \delta\phi]_m$ is displayed here as a vector to simplify the indexing. Discretizing the integral equation in one dimension, with a fixed step size $\Delta x' = (b - a)/N$, makes it apparent that the discretized equation is a linear matrix equation in the form of

$$\left(I - iG\boldsymbol{\Sigma}^I \Delta x\right) \boldsymbol{\delta\phi} = G\boldsymbol{\delta S}\Delta x, \tag{2.20}$$

where Δx is a constant step size, and can easily be solved numerically. The Green's function is defined as:

$$G = \begin{bmatrix} G_{1\to 1} & G_{2\to 1} \\ G_{1\to 2} & G_{2\to 2} \end{bmatrix}, \tag{2.21}$$

and the perturbation, $\boldsymbol{\delta S}$, and the imaginary cross-section matrix, $\boldsymbol{\Sigma}^I$, are defined as before in equations (2.8) and (2.11), respectively.

The discretization in two dimensions is done similarly to [13]. Analogously as for the one dimensional case the integral equation, in the domain $A \in [a, b] \times [c, d]$ with a square mesh size of $N \times N$, becomes

$$\left(I - iG\boldsymbol{\Sigma}^I \Delta x \Delta y\right) \boldsymbol{\delta\phi} = G\boldsymbol{\delta S}\Delta x \Delta y, \tag{2.22}$$

where I is the identity matrix and $\Delta x = (b - a)/N$, $\Delta y = (d - c)/N$. The discrete Green's function is defined as $G_{g\to g'}(x, y, x', y') = G_{g\to g' iljm}$, with i, l, j, m corresponding to x, y, x', y', respectively, resulting in the Green's function

$$G_{g\to g'} = \begin{bmatrix} G^{(1,1)}_{g\to g'} & G^{(1,2)}_{g\to g'} & \dots & G^{(1,N)}_{g\to g'} \\ G^{(2,1)}_{g\to g'} & G^{(2,2)}_{g\to g'} & \dots & G^{(2,N)}_{g\to g'} \\ \vdots & \vdots & \ddots & \vdots \\ G^{(N,1)}_{g\to g'} & \dots & \dots & G^{(N,N)}_{g\to g'}, \end{bmatrix} \tag{2.23}$$

and $G^{(i,j)}_{g\to g'} = [G_{g\to g' iljm}]^N_{l,m=1}$, where the entire matrix, of the size $2N^2 \times 2N^2$, is given by

$$G = \begin{bmatrix} G_{1\to 1} & G_{2\to 1} \\ G_{1\to 2} & G_{2\to 2} \end{bmatrix}. \tag{2.24}$$

The cross-section matrix, $\boldsymbol{\Sigma}^{I,2D}$, is defined, by splitting the cross-section matrix, for the one dimensional case, into its sub-matrices, as

$$\boldsymbol{\Sigma}^{I,1D} = \begin{bmatrix} \boldsymbol{\Sigma}^I_{1,1} & \boldsymbol{\Sigma}^I_{1,2} \\ \mathbf{0} & \boldsymbol{\Sigma}^I_{2,2} \end{bmatrix} \tag{2.25}$$

$$\mathbf{\Sigma}^{I,2D} = \begin{bmatrix} I \otimes \mathbf{\Sigma}^I_{1,1} & I \otimes \mathbf{\Sigma}^I_{1,2} \\ \mathbf{0} & I \otimes \mathbf{\Sigma}^I_{2,2} \end{bmatrix}, \tag{2.26}$$

where $\mathbf{\Sigma}^{I,1D}$ is defined in the same way as the one dimensional case and $\otimes$ is the Krönecker product that multiplies every element of the left matrix with the whole right matrix, and the dynamic flux and noise source are defined as vectors in the form $[\delta\phi]^N_{i,j=1}$ and $[\delta S]^N_{i,j=1}$.

2.4 Relating $G_{1\to g'}$ and $G_{2\to g'}$ Simulations Through their Source Strengths

The Green's components of (2.12) are determined with two different simulations, one for $g = 1$ and one for $g = 2$, and therefore they are not directly related to each other. However, since they have the same source strength (equal to unity), they can be normalized according to the source position. This method of normalization is chosen because of the fact that if all parameters in a system are known, the solution for a source calculation is unique and no external quantity is needed (as the power for normalization of the static flux calculation). In one dimension, this can be achieved by integrating the top equation of (2.12) and the bottom equation of (2.13) on a small length, ϵ, around the source point. The following relations are then obtained:

$$\lim_{\epsilon\to 0} N_{11}(x')D_1(x') \left[\frac{\mathrm{d}}{\mathrm{d}x}G_{1\to 1}\right]^{x'+\epsilon}_{x'-\epsilon} = -1 \tag{2.27}$$

$$\lim_{\epsilon\to 0} N_{22}(x')D_2(x') \left[\frac{\mathrm{d}}{\mathrm{d}x}G_{2\to 2}\right]^{x'+\epsilon}_{x'-\epsilon} = -1, \tag{2.28}$$

where N_{11} is the amplitude of $G_{1\to 1}$ and N_{22} is the amplitude of $G_{2\to 2}$. In two dimensions the source strength is obtained integrating around the source. Using the divergence theorem on the left hand side results in

$$\lim_{\epsilon\to 0} N_{11}(x',y')D_1(x',y') \left(\left[\frac{\partial}{\partial x}G_{1\to 1}\right]^{x'+\epsilon}_{x'-\epsilon} + \left[\frac{\partial}{\partial y}G_{1\to 1}\right]^{y'+\epsilon}_{y'-\epsilon}\right) = -1 \tag{2.29}$$

$$\lim_{\epsilon\to 0} N_{22}(x',y')D_2(x',y') \left(\left[\frac{\partial}{\partial x}G_{2\to 2}\right]^{x'+\epsilon}_{x'-\epsilon} + \left[\frac{\partial}{\partial y}G_{2\to 2}\right]^{y'+\epsilon}_{y'-\epsilon}\right) = -1, \tag{2.30}$$

The amplitudes N_{12} and N_{21} are given by

$$N_{12}(\mathbf{r}') = N_{11}(\mathbf{r}')\frac{\max_{\mathbf{r}'} G_{1\to 2}}{\max_{\mathbf{r}'} G_{1\to 1}} \tag{2.31}$$

$$N_{21}(\mathbf{r}') = N_{22}(\mathbf{r}')\frac{\max_{\mathbf{r}'} G_{2\to 1}}{\max_{\mathbf{r}'} G_{2\to 2}}, \tag{2.32}$$

since $G_{1\to 1}$ and $G_{1\to 2}$ or $G_{2\to 1}$ and $G_{2\to 2}$ come from the same simulation and are already related to each other, they only need to be re-normalized according to N_{11} or N_{22}, respectively.

Note that the normalization is done according to diffusion theory and not transport theory which Monte Carlo is based on. For a potentially better result of the normalization, the discontinuity of the neutron current at the source point should be used, that is equation (2.27) is replaced by

$$\lim_{\epsilon \to 0} N_{11}(x') \left[\boldsymbol{J}_{1 \to 1} \right]_{x'-\epsilon}^{x'+\epsilon} = 1. \tag{2.33}$$

This, however, has proven to be cumbersome for the automation of the simulations, because of the structure of the output file of MCNP.

3
Method

3.1 Implementation

The Monte Carlo-based noise method can be implemented in the following way. Once the geometry and materials have been chosen, a set of homogenized cross sections that resembles two-group diffusion theory are calculated from a Monte Carlo simulation, according to [2, 9], and an ACE-file (A Compact Evaluated nuclear data file) [10] is created with these new cross sections. The cross-sections that are inputted in the ACE-file in this case are macroscopic and are used in MCNP by inserting a material density of 1 particle/barn $\cdot$ cm. The cross-sections and quantities used in the custom ACE-files are the macroscopic transport cross-section Σ_{tr}, non-elastic scattering cross section Σ_s, macroscopic absorption Σ_a, macroscopic fission cross-section Σ_f, average neutron yield ν, and fission spectrum χ which is not included in table 3.1 since only fast neutrons are produced in this case. The cut-off between energy groups is set at 0.625 eV. The diffusion coefficient for comparison with diffusion based code is defined as $D = 1/3\Sigma_{tr}$.

When the cross-sections are known, a criticality simulation is performed, with the two-group cross sections in Monte Carlo to estimate k_{eff} and the static flux. With this estimated multiplication factor, the average neutron yields are updated with the factor (2.17). Note that the neutron yields are updated and not the fission cross-section, since the fission, absorption and capture cross-sections in the ACE-files are dependent on each other, whereas only one value changes if the neutron yield of a group is updated.

The Green's function (2.12) is determined with Monte Carlo by substituting the Dirac deltas on the right side with volumetric sources that cover the unit mesh volumes, that is the source strength is divided by the unit mesh volume. When integrating on the mesh size, the source strength is multiplied by the unit mesh volume and the source strength after integration is independent of the mesh size. Two simulations are performed per mesh volume, one with a fast source that determines $G_{1\to1}$ & $G_{1\to2}$ and one with a thermal source that determines $G_{2\to1}$ & $G_{2\to2}$.

When the Green's function is determined, then all the needed information is known, and the dynamic flux is obtained by solving the matrix equation (2.20).

The methodology for Monte Carlo-based noise calculation is summarised in six steps:

1. Choose geometry & material for the system.
2. Determine the corresponding two-group cross sections for Monte Carlo.
3. Perform a static criticality simulation to estimate k_{eff}, $\boldsymbol{\phi}_0$.
4. Update the average neutron yields according to:
   $\nu_{new} = \nu_{old}/k_{eff} \cdot (\lambda^2 + \omega^2(1-\beta))/(\lambda^2 + \omega^2)$.
5. Determine the systems Green's function with two source simulation at each mesh volume.
6. Solve the matrix equation (2.20) to determine the neutron flux fluctuation $\boldsymbol{\delta\phi}$.

3.2 Verification

Three geometries are considered hereafter. A homogeneous slab reactor between $x = \pm 100.5\,\text{cm}$ with vacuum boundaries (see figure 3.1) to demonstrate validity of the method, a one dimensional system of eleven 1 cm thick fuel pins with a 0.25 cm thick layer of water as moderator between each fuel pin and 0.125 cm thick layer of water between the end fuel pins with vacuum boundary (see figure 3.2) to show that the presented method can handle complex geometries, and a two dimensional homogeneous square reactor of $101 \times 101\,\text{cm}^2$ with vacuum boundaries (see figure 3.3) to illustrate that the method can be extended to higher dimensions.

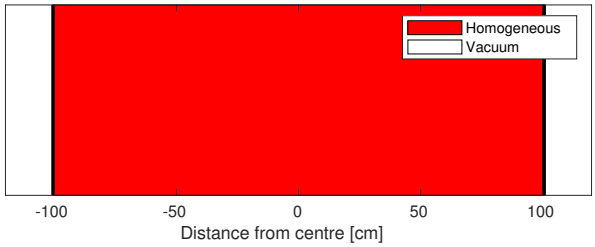

Figure 3.1: One dimensional 201 cm wide homogeneous slab reactor with vacuum boundaries.

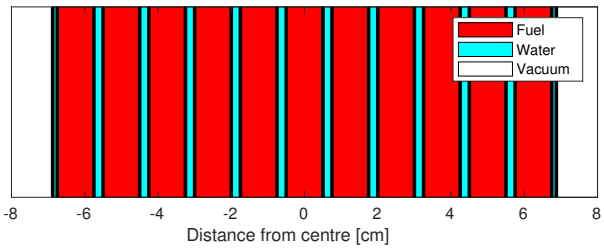

Figure 3.2: One dimensional reactor with eleven 1 cm wide fuel pins with 0.25 cm thick layer of light water between the fuel pins as moderator and 0.125 cm thick layer of light water between the fuel pins and vacuum boundaries.

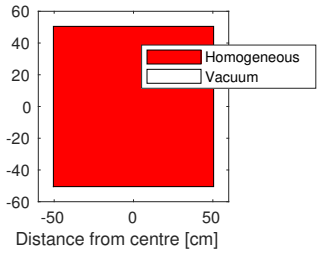

Figure 3.3: Two dimensional $101 \times 101\,\mathrm{cm}^2$ square slab reactor with vacuum boundaries.

The parameters for both systems are given in table 3.1 and the point-kinetic data, as well as the perturbations, are given in table 3.2. The frequencies that are analyzed are those at the cut-off regions and frequencies on the plateau region for the respective systems.

Material properties	Fuel region	Mod region	Homogeneous
$\Sigma_{a,1,0}$	$0.0188\ \mathrm{cm}^{-1}$	$4 \cdot 10^{-4}\ \mathrm{cm}^{-1}$	$0.0157\ \mathrm{cm}^{-1}$
$\Sigma_{a,2,0}$	$0.1451\ \mathrm{cm}^{-1}$	$0.0206\ \mathrm{cm}^{-1}$	$0.1202\ \mathrm{cm}^{-1}$
$\Sigma_{f,1,0}$	$0.00472\ \mathrm{cm}^{-1}$	-	$3.775 \cdot 10^{-3}\ \mathrm{cm}^{-1}$
$\Sigma_{f,2,0}$	$0.10045\ \mathrm{cm}^{-1}$	-	$0.0804\ \mathrm{cm}^{-1}$
ν_1	2.5636	-	2.5636
ν_2	2.4367	-	2.4367
$\Sigma_{r,0}$	$2.3 \cdot 10^{-4}\ \mathrm{cm}^{-1}$	$0.0135\ \mathrm{cm}^{-1}$	$0.0029\ \mathrm{cm}^{-1}$
$\Sigma_{tr,1}$	$0.4117\ \mathrm{cm}^{-1}$	$0.2865\ \mathrm{cm}^{-1}$	$0.3866\ \mathrm{cm}^{-1}$
$\Sigma_{tr,2}$	$0.5590\ \mathrm{cm}^{-1}$	$1.0434\ \mathrm{cm}^{-1}$	$0.6558\ \mathrm{cm}^{-1}$
$D_{1,0}$	0.8096 cm	1.1635 cm	0.8620 cm
$D_{2,0}$	0.5964 cm	0.3195 cm	0.5083 cm

Table 3.1: Cross section data for fuel and moderator, or for the homogeneous region. Data taken from [1].

Point-Kinetic Data		Perturbation	Strength
β	530 pcm	$\delta\nu\Sigma_{f,i}$	$2S\ \mathrm{cm}^{-1}$
λ	$0.0851\ \mathrm{s}^{-1}$	$\delta\Sigma_{a,i}$	$S\ \mathrm{cm}^{-1}$
v_1	$1.52 \cdot 10^7$ cm/s	$\delta\Sigma_r$	$S\ \mathrm{cm}^{-1}$
v_2	$4.13 \cdot 10^5$ cm/s	Arbitrary noise source	$S \in \mathbb{C}$

Table 3.2: Point-kinetic data and perturbation strengths ($i = 1, 2$ for fast and thermal groups, respectively.)

System	MCNP k_{eff}	CORE SIM k_{eff}
Homogeneous	0.76548 ± 0.00031	0.76401
11 Fuel Pin	0.30171 ± 0.00002	0.29022
2D Homogeneous	0.71171 ± 0.00017	0.70992

Table 3.3: Multiplication factors for the different systems analyzed.

3.3 Symmetries

For the one-dimensional cases, the source calculations were performed for the right half side of the space while the flux was estimated throughout the whole system, and then the Green's function was mirrored in order to save computational time. The estimated Green's function is denoted $G^{1/2}_{g\to g',ij}$ where $i = 1, 2, \ldots, I$ and $j = J/2, J/2+1, \ldots, J$, where i represents the flux position and j the source position. The right side of the sources was mirrored onto the left side according to

$$G^{1/2}_{g\to g',ij} = G_{g\to g',I-i,J-j}. \tag{3.1}$$

For the two dimensional system, the source calculations were performed for the top right quarter of the geometry while the flux was estimated throughout the whole system. This was done in order to save computational time. The Green's function is denoted by $G^{1/4}_{ijkl}$, where ij are the flux positions, $i = 1, \ldots, I$ and $j = 1, \ldots, J$, while kl are the source positions $k = K/2, ...K$ and $l = L/2, ...L$. The top right quarter of the sources were mirrored to the top left, bottom left, and bottom right according to

$$\begin{aligned} G^{1/4}_{g\to g',ijkl} &= G_{g\to g',I-i,j,K-k,l} \\ G^{1/4}_{g\to g',ijkl} &= G_{g\to g',I-i,J-j,K-k,L-l} \\ G^{1/4}_{g\to g',ijkl} &= G_{g\to g',i,J-j,k,L-l}, \end{aligned} \tag{3.2}$$

respectively.

Generally, the thermal source will generate more neutrons since neutrons from the fast source escape before being thermalized. Therefore, it is advisable to use fewer neutrons when determining $G_{2\to g'}$. Before the source calculations are started, it is also recommended to perform a simulation at a point near the middle of the system where most of the neutrons are created and a point near the boundary where fewer neutrons are created, as well as both fuel and moderator regions to get a sense of the upper and lower time duration for the whole simulation.

4

Results

In the following, three types of simulations are presented: direct CORE SIM simulation, Monte Carlo based simulation, and the same methodology as presented in this report but with CORE SIM used to determine the Green's function.

The validity of the method is shown in figure 4.1, where CORE SIM was used to determine the Green's function and then compared with a direct CORE SIM simulation. The Green's functions were calculated at three different step sizes, and all of them overlap which means that the method is insensitive to the step size.

Figure 4.2 compares direct CORE SIM with four different Green's functions, calculated with CORE SIM, fixed at different frequencies. The Green's functions fixed at frequencies at the plateau region and above show little difference while the Green's function fixed at the lower frequency cut-off causes a deviation from the direct CORE SIM simulation when trying to calculate frequency at the plateau. Figure 4.3 compares the amplitude and phase of the fast flux as a function of frequency of CORE SIM and the MCNP based method with a Green's function fixed at a frequency of $1/2\pi$ Hz. The MCNP based method has similar behaviour as CORE SIM at the plateau region. In this region, the phase at all points of the system is closer to zero than CORE SIM, while the phase according to CORE SIM is greater for an interval above the upper frequency cut-off. This demonstrates that noise simulations at low frequencies are no longer reliable if the frequency for the Green's is fixed at the plateau region or above.

Figures 4.4, 4.5, 4.6 and 4.7 show the difference between CORE SIM and the Monte-Carlo based method with different mesh sizes for the homogeneous system. A finer mesh in MCNP results in a distribution and phase that more closely resembles the results from CORE SIM, where a finer mesh is required in MCNP than in CORE SIM to reach mesh convergence. Similar frequency dependence is observed for the heterogeneous 11 fuel pin system as seen in figures 4.8 and 4.9. The response for the MCNP based method is faster than CORE SIM at the plateau, while the opposite is true for the eleven fuel pins system at high frequencies where the behaviour differs, around the upper cut-off frequency, compared to the homogeneous case. The phase at this upper cut-off frequency according to CORE SIM is larger than the Monte Carlo-based method.

The dynamic calculations for the two dimensional square reactor are displayed in figures 4.10, 4.11, 4.12 and 4.13. For all frequencies, the MCNP based method has a larger phase than the phase given by CORE SIM. The absolute difference between CORE SIM and the MCNP based method, for the 185 Hz, is $\sim$0.07 rad for the fast phase and $\sim$0.04 rad for the thermal phase. The step size for the MCNP simulation is 1 cm. The one-dimensional case suggests that this mesh size is not fine enough

for the solution to be mesh independent. Observations from the one dimensional homogeneous case suggest that a finer mesh results in a smaller phase.

Although not presented in any of the figures, when the Green's function is obtained with CORE SIM, for either low or high frequencies, the resulting flux distribution is indistinguishable from a direct CORE SIM simulation. It is unclear whether the differences observed between MCNP and CORE SIM, for low frequencies, in this regard is a result from the difference between transport and diffusion, or due an issue of implementation in the Monte Carlo-based method.

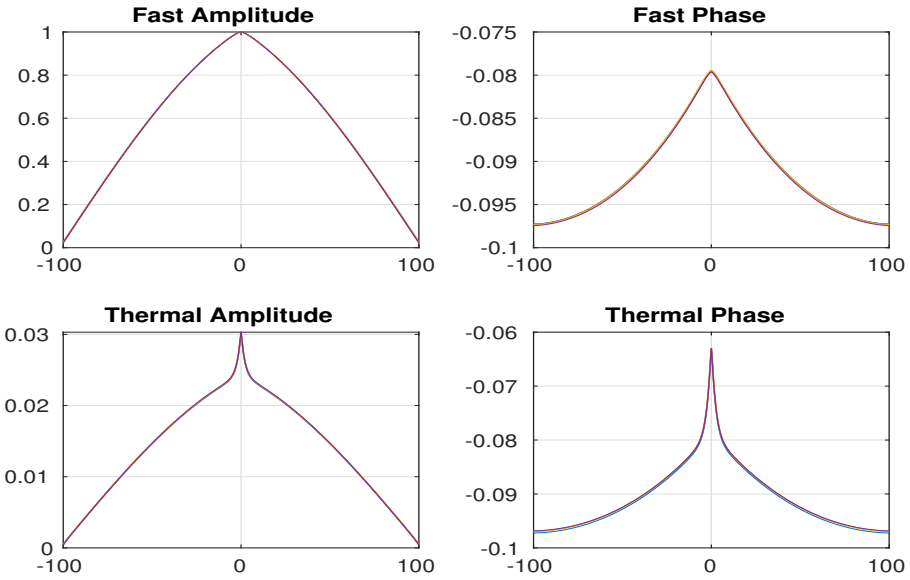

Figure 4.1: Homogeneous system with perturbation in the middle with a frequency of $1/2\pi$ Hz to show the validity of the method through comparison with CORE SIM (blue), with the step size 0.25 cm, and three Green's functions, calculated with CORE SIM, with varying step size 1 cm (red), 0.33 cm (yellow) and 0.25 cm (purple). The $x-$axis displays the distance from the centre of the core, the $y-$axis the amplitude of the flux relative to the max value in the fast group (left) and the $y-$axis the phase in radians (right).

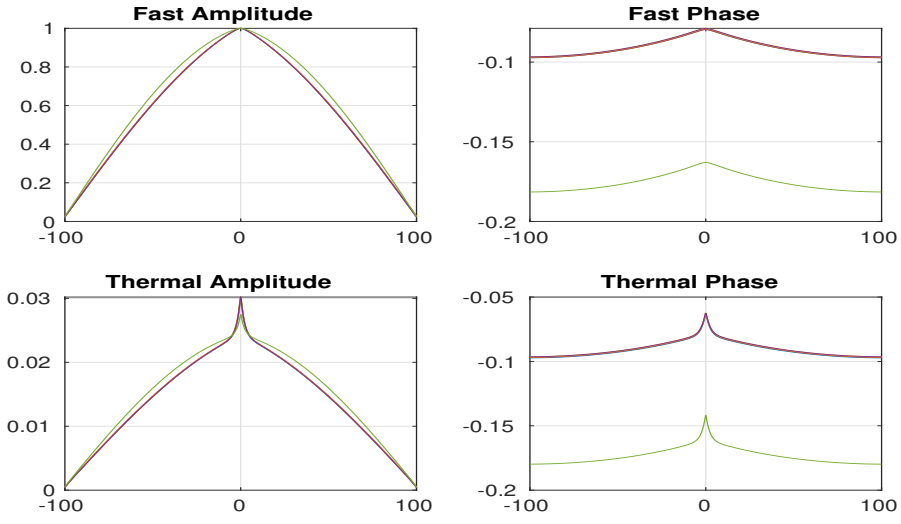

of

Figure 4.2: Homogeneous system with perturbation in the middle at a frequency of $1/2\pi$ Hz calculated with CORE SIM directly (blue) and four different Green's functions from CORE SIM fixed at four different frequencies, 0.0135 Hz (green), $1/2\pi$ Hz (red), $10/2\pi$ Hz (yellow) and ∞ Hz (purple). The $x-$axis displays the distance from the centre of the core, the $y-$axis the amplitude shows the flux relative to the max value in the fast group (left) and the $y-$axis the phase in radians (right).

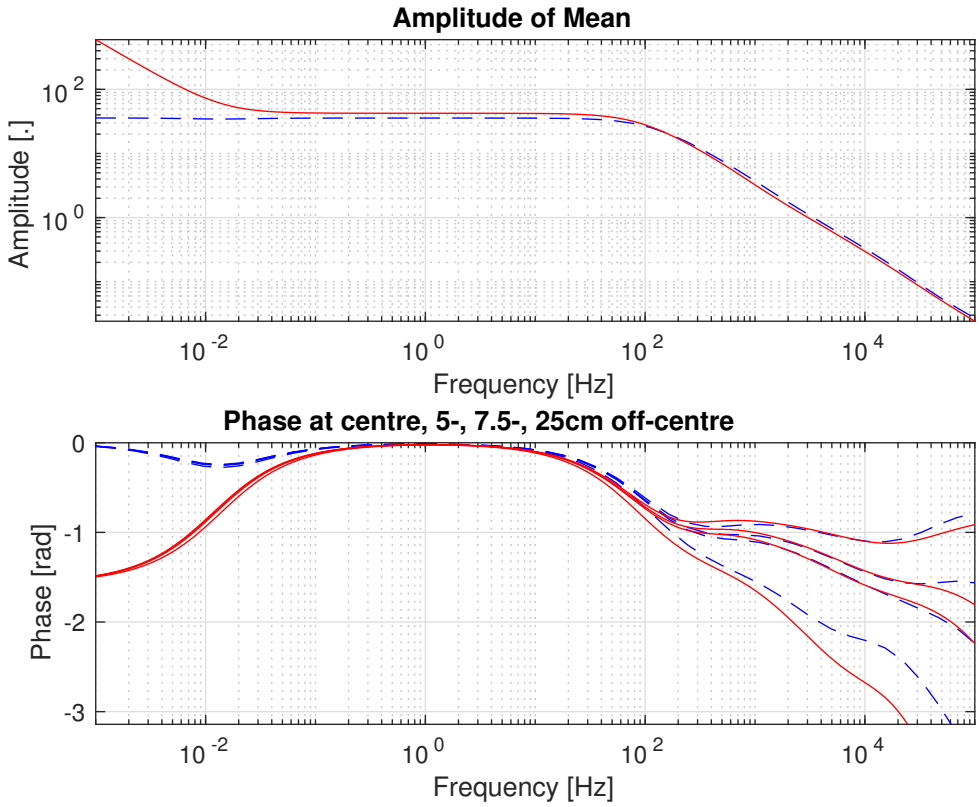

Figure 4.3: Mean amplitude/Phase of the fast flux for the homogeneous system, with a perturbation at the centre, as a function of frequency with a step size of 0.25 cm. The red graphs are simulated with CORE SIM and the dashed blue graphs are estimated with the Monte Carlo-based method with a Green's function fixed at a frequency of $1/2\pi$ Hz. The phase is collected a four points: the centre, 5 cm off-centre, 7.5 cm off-centre and 25 cm off-centre.

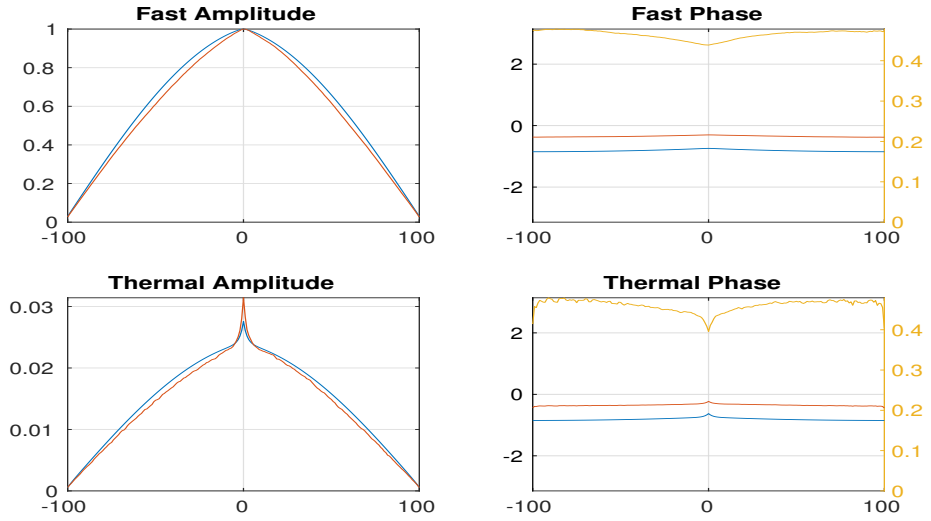

Figure 4.4: Homogeneous system with a frequency of 0.0135 Hz, with a step size of 1 cm. MCNP-based simulations (red) are compared with CORE SIM (blue), and the yellow graph in the phase plots displays the absolute difference of the phase in radians, between CORE Sim and Monte Carlo. The $x-$axis displays the distance from the centre of the core, the $y-$axis the amplitude of the flux relative to the max value in the fast group (left) and the $y-$axis the phase in radians (right).

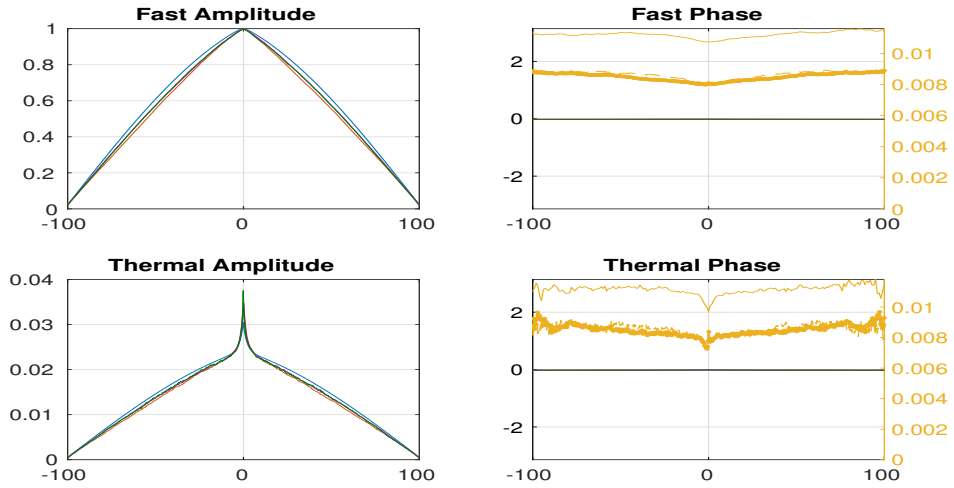

Figure 4.5: Homogeneous system with flux frequency at 1 Hz and Green's function fixed at $1/2\pi$ Hz, where the Green's functions is calculated with MCNP with different step sized, 1 cm (red), 0.33 cm (purple), and 0.25 cm (green), compared with CORE SIM (blue). The right axis on the phase graphs displays the absolute difference between the Monte Carlo method and CORE SIM, where the solid line represents step size 1 cm, the dotted line step size 0.33 cm, the dashed line step size 0.25 cm. The $x-$axis displays the distance from the centre of the core, the $y-$axis the amplitude of the flux relative to the max value in the fast group (left) and the $y-$axis the phase in radians (right).

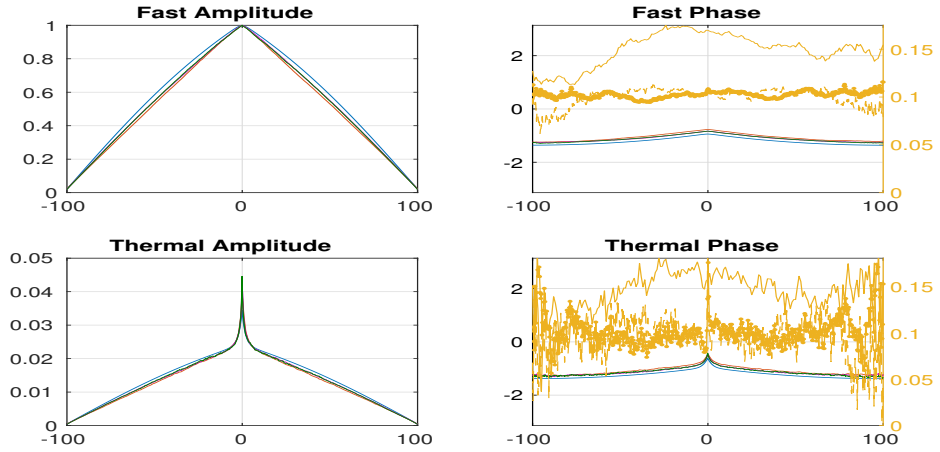

Figure 4.6: Homogeneous system at a frequency of 185 Hz and a Green's function fixed at a frequency of $1/2\pi$ Hz, where the Green's functions are calculated with MCNP with different step sizes, 1 cm (red), 0.33 cm (purple), and 0.25 cm (green). The CORE SIM simulaiton is represented in blue. The right axis on the phase graphs displays the absolute difference between the Monte Carlo method and CORE SIM, where the solid line represents step size 1 cm, the dotted line step size 0.33 cm, the dashed line step size 0.25 cm. The $x-$axis displays the distance from the centre of the core, the $y-$axis the amplitude of the flux relative to the max value in the fast group (left) and the $y-$axis the phase in radians (right).

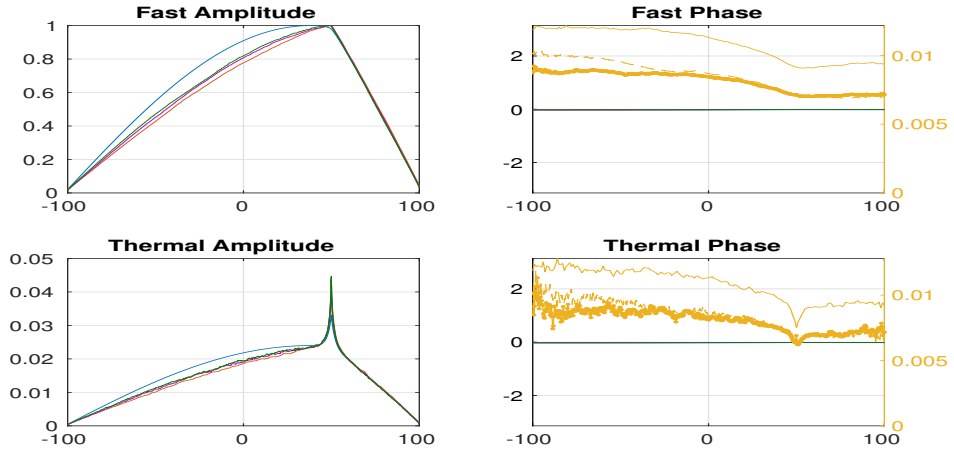

Figure 4.7: Homogeneous system with a frequency of 1 Hz and Green's function fixed at a frequency of $1/2\pi$ Hz with a perturbation 50 m off-centre, where the Green's functions are calculated with MCNP with different step sizes, 1 cm (red) and 0.25 cm (green), compared with CORE SIM (blue). The right axis on the phase graphs displays the absolute difference between the Monte Carlo method and CORE SIM, where the solid line represents step size 1 m, the dotted line step size 0.33 cm, and the dashed line 0.25 cm. The $x-$axis displays the distance from the centre of the core, the $y-$axis the amplitude of the flux relative to the max value in the fast group (left) and the $y-$axis the phase in radians (right).

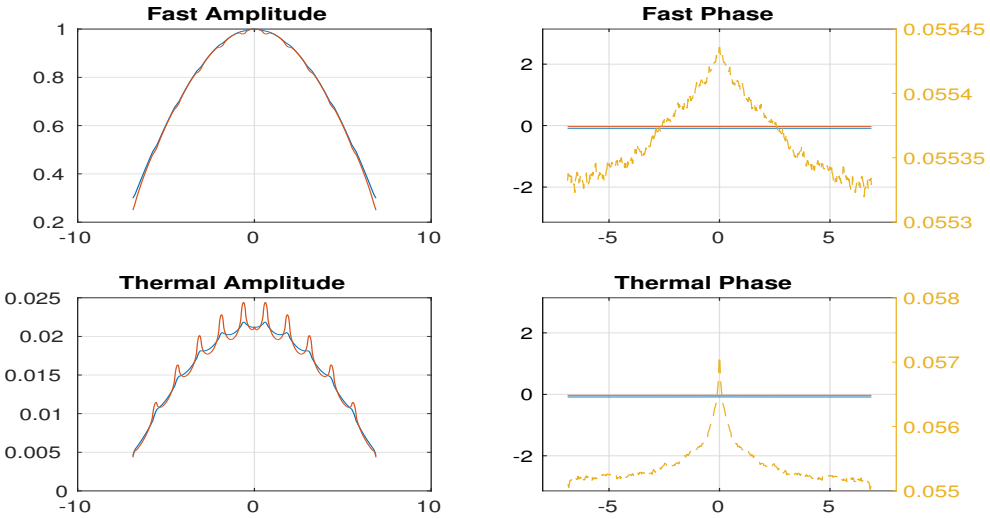

Figure 4.8: 11 fuel pin system with a frequency of $1/2\pi$ Hz. Comparison with CORE SIM (blue), and MCNP (red), with a step size in MCNP of 0.025 cm. The $x-$axis displays the distance from the centre in cm, the $y-$axis on the amplitude graphs (left) are normalised according to the maximum value of the fast flux. The left $y-$axis on the phase graphs (right) are in radians while the right $y-$axis shows the absolute difference between the phases of CORE SIM and MCNP in radians.

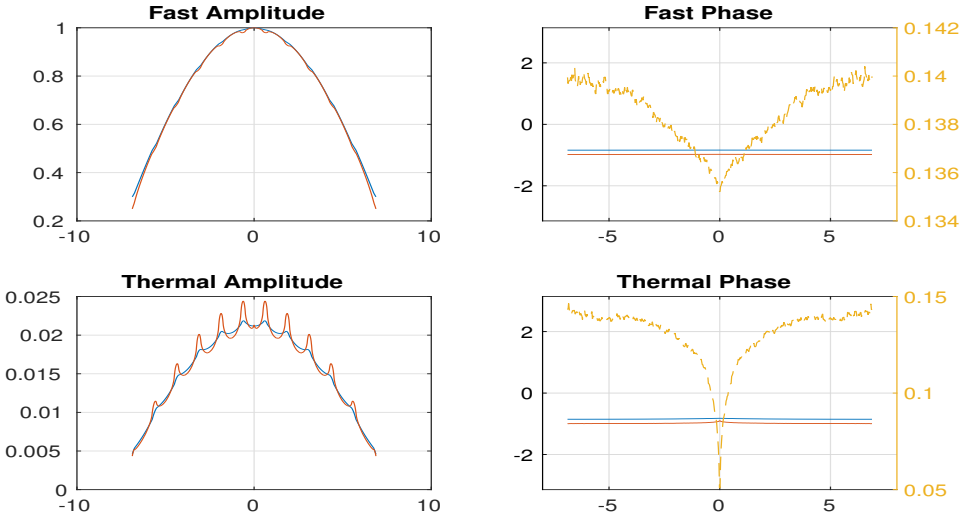

Figure 4.9: 11 fuel pin system with a frequency of 150 Hz and a Green's function fixed at a frequency of $1/2\pi$ Hz. Comparison with CORESIM (blue), and MCNP (red), with a step size in MCNP of 0.025 cm. The $x-$axis displays the distance from the centre in cm, the $y-$axis on the amplitude graphs (left) are normalised according to the maximum value of the fast flux. The left $y-$axis on the phase graphs (right) are in radians while the right $y-$axis shows the absolute difference between the phases of CORE SIM and MCNP in radians.

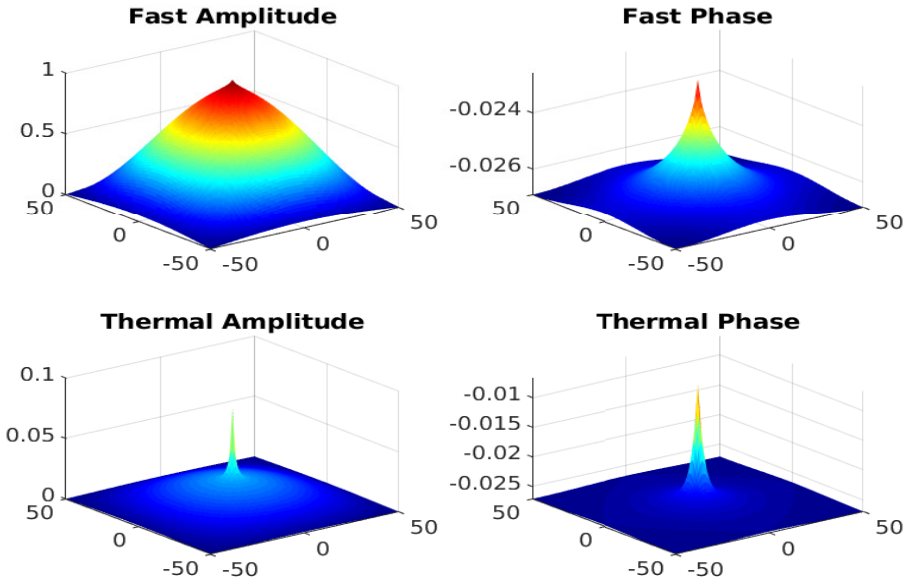

Figure 4.10: CORE SIM simulation of two dimensional homogeneous reactor with a frequency of $10/2\pi$ Hz, with perturbation at the centre. The base axis displays the distance from the centre, the $z-$axis of the amplitude (left) is normalised according to the maximum of the fast amplitude, and the $z-$axis of the phase (right) is displayed in radians.

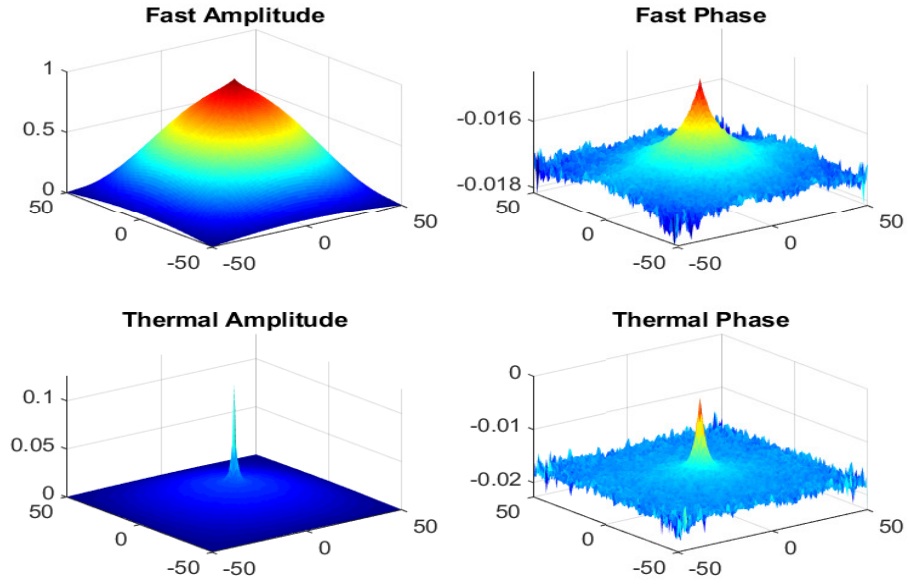

Figure 4.11: MCNP based simulation of two dimensional homogeneous reactor with a frequency of $10/2\pi$ Hz, with perturbation at the centre. The base axis displays the distance from the centre, the $z-$axis of the amplitude (left) is normalised according to the maximum of the fast amplitude, and the $z-$axis of the phase (right) is displayed in radians.

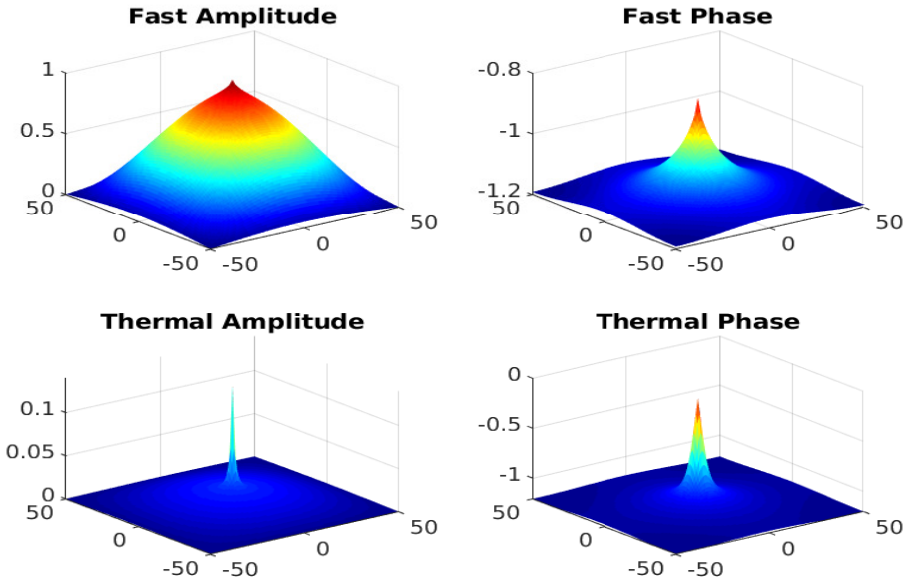

Figure 4.12: CORE SIM simulation of two dimensional homogeneous reactor with a frequency of 185 Hz, with perturbation at the centre. The base axis displays the distance from the centre, the $z-$axis of the amplitude (left) is normalised according to the maximum of the fast amplitude, and the $z-$axis of the phase (right) is displayed in radians.

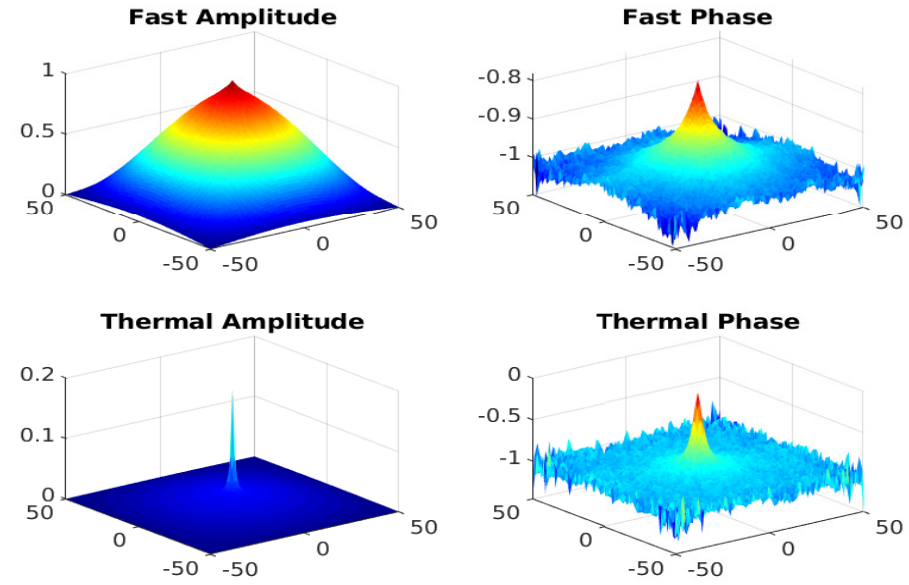

Figure 4.13: MCNP based simulation of two dimensional homogeneous reactor with a frequency of 185 Hz and a Green's function fixed at a frequency of $10/2\pi$ Hz, with perturbation at the centre. The base axis displays the distance from the centre, the $z-$axis of the amplitude (left) is normalised according to the maximum of the fast amplitude, and the $z-$axis of the phase (right) is displayed in radians.

5
Conclusion

An approach has been developed to perform dynamic calculations based on a Monte-Carlo without any modification to the source code, by splitting the cross-sections into their real and imaginary parts and acting upon the real values as if they represented a static sub-critical system with an external source while treating the imaginary values as an additional perturbation.

The results agree well with the results from CORE SIM concerning the amplitude and phase at the plateau region, while the behaviour of the two methods differ slightly at frequencies near the upper cut-off frequency and above. MCNP requires a finer mesh to achieve mesh convergence compared to CORE SIM. The same Green's function estimated at a given frequency within the range of the plateau region and above can be used to calculate the dynamic flux with negligible errors, thus demonstrating the versatility of the method.

In contrast to the previous work [2, 1], the method proposed here is applicable to all frequencies and all noise sources. Based on the comparison with CORE SIM, the method presented in this report result in a sharper flux distribution, which is to be expected by transport theory.

Bibliography

[1] E. E. Pettersen, C. Demazière, K. Jareteg, T. Schnfeldt, E. Nonbøl, and Bent Lauritzen. Development of a Monte-Carlo based method for calculating the effect of stationary fluctuations. In *Mathematics and Computations, Supercomputing in Nuclear Applications and Monte Carlo International Conference (M&C+SNA+MC 2015)*, 2015.

[2] E. E. Pettersen. Calculation of dynamic reactor systems with stochastic neutronic code MCNP5, 2014. Bacherlor's thesis.

[3] Imre Pázsit and Christophe Demazière. Noise techniques in nuclear systems. In *Handbook of Nuclear Engineering*, volume 3. SPRINGER NATURE, 2010.

[4] DEMAZIÈRE C. Development of a 2-d 2-group neutron noise simulator. *Ann. Nucl. Energy*, 31:647, 2004.

[5] Christophe Demazière. CORE SIM: A multi-purpose neutronic tool for research and education. *Annals of Nuclear Energy*, 38(12):2698 – 2718, 2011.

[6] MALMIR H., VOSOUGHI N., and ZAHEDINEJAD E. Development of a 2-d 2-group neutron noise simulator for hexagonal geometries. *Ann. Nucl. Energy*, 37:1089, 2010.

[7] V. Larsson and Christophe Demazière. Comparative study of 2-group P1 and diffusion theories for the calculation of neutron noise in 1D 2-region systems. *Annals of Nuclear Energy*, 36(10):1574 – 1587, 2009.

[8] Hoai Nam Tran and Christophe Demazière. Neutron noise calculations in hexagonal geometry and comparison with analytical solutions. *Nuclear Science and Engineering*, 175(3):340–351, 2013.

[9] J. C. Kuijper, S. C. van der Marck, and A. Hogenbirk. Using homogenized macroscopic group cross-section in continuous-energy Monte Carlo neutron transport calculations with MCNP. In *Proceedings of Joint International Topuical Meeting on Mathematics & Computation and Supercomputing in Nuclear Applications (M&C+SNA+MC 2017)*, 03 2007.

[10] C. J. Werner(editor). *MCNP Users Manual - Code Version 6.2*. Los Alamos National Laboratory, report la-ur-17-29981 edition, 2017.

[11] Jaakko Leppänen, Maria Pusa, Tuomas Viitanen, Ville Valtavirta, and Toni Kaltiaisenaho. The serpent monte carlo code: Status, development and applications in 2013. *Annals of Nuclear Energy*, 82:142 – 150, 2015. Joint International Conference on Supercomputing in Nuclear Applications and Monte Carlo 2013, SNA + MC 2013. Pluri- and Trans-disciplinarity, Towards New Modeling and Numerical Simulation Paradigms.

[12] Jaakko Leppänen. Private communication, 2019.

[13] Wen-Jing Xie and Fu-Rong Lin. A fast numerical solution method for two dimensional fredholm integral equations of the second kind. *Applied Numerical Mathematics*, 59(7):1709 – 1719, 2009.